Retardation of Proton Transfer Caused by Binding of the Transition Metal Ion to the Bacterial Reaction Center Is Due to pK_a Shifts of Key Protonatable Residues[†]

László Gerencsér and Péter Maróti*

Department of Biophysics, University of Szeged, P.O. Box 655, 6701 Szeged, Hungary

Received September 14, 2000; Revised Manuscript Received November 28, 2000

ABSTRACT: Transition metal ions bind to the reaction center (RC) protein of the photosynthetic bacterium *Rhodobacter sphaeroides* and slow the light-induced electron and proton transfer to the secondary quinone, Q_B. We studied the properties of the metal ion−RC complex by measuring the pH dependence of the dissociation constant and the stoichiometry of proton release upon ligand formation. We investigated the mechanism of inhibition by measuring the stoichiometry and kinetics of flash-induced proton binding, the transfer of (first and second) electrons to Q_B, and the rate of steady-state turnover of the RC in the absence and presence of Cd^{2+} and Ni^{2+} on a wide pH range. The following results were obtained. (1) The complexation of transition metal ions Cd^{2+} and Ni^{2+} with the bacterial RC showed strong pH dependence. This observation was explained by different (pH-dependent) states of the metal−ligand cluster: the complex formation was strong when the ligand (Asp and His residues) was deprotonated and was much weaker if the ligand was partly (or fully) protonated. A direct consequence of the model was the pH-dependent proton release upon complexation. (2) The retardation of transfer of electrons and protons to Q_B was also strongly pH-dependent. The effect was large in the neutral pH range and decreased toward the acidic and alkaline pH values. (3) Steady-state turnover measurements indicated that the rate of the second proton transfer was much less inhibited than that of the first one, which became the rate-limiting step in continuous turnover of the RC. (4) Sodium azide partly recovered the proton transfer rate. The effect is not due to removal of the bound metal ion by azide but probably by formation of a proton-transporting azide network similarly as water molecules may build up proton pathways. (5) We argue that the inhibition comes mainly from pK_a shifts of key protonatable residues that control the proton transfer along the H-bond network to Q_B. The electrostatic interaction between the metal ion and these residues may result in acidic pK_a shifts between 1.5 and 2.0 that account for the observed retardation of the electron and proton transfer.

Transmembrane proton transport in photosynthetic bacteria is coupled to light-induced electron transfer (ET)[1] in the reaction center (RC) through a series of electron donor and acceptor molecules (see ref *1* for reviews). The charge separation is initiated by flash excitation of the bacteriochlorophyll dimer, P ($P \rightarrow P^*$) followed by three sequential ET reactions to bacteriopheophytin, I ($P^* \rightarrow P^+I^-$), primary quinone, Q_A ($P^+I^- \rightarrow P^+Q_A^-$), and secondary quinone, Q_B ($P^+Q_A^- \rightarrow P^+Q_B^-$) that take place on the few picosecond, hundred picosecond, and hundred microsecond time scales, respectively. If the external electron donor (cyt c^{2+}) is available on the donor side, then it can rereduce the oxidized dimer

$$P^+ \text{ cyt } c^{2+} \rightarrow P \text{ cyt } c^{3+} \quad (1)$$

and similarly ET from P to Q_B^- can be initiated by additional flash excitation. The ET reactions on the acceptor side are more complicated than on the donor side because they are coupled to changes in conformational and in protonational states of the RC (*2*−*4*). The first interquinone ET to Q_B can occur only after conformational gating (*5*−*7*) and does not involve direct protonation of the quinone in the isolated RC in the physiological pH range (*5*, *8*−*10*):

$$Q_A^-Q_B(\text{inactive}) \xrightarrow{\text{conformational gating}} Q_A^-Q_B \xrightarrow{\text{first electron}} Q_AQ_B^- \quad (2)$$

The conformational gating can include the movement of Q_B from the distal to the proximal position in the binding pocket (*11*), protein dynamics (*12*), or proton transfer (*9*). The accompanied pH-dependent substoichiometric amount of proton uptake is due to pK changes of protonatable amino acid residues nearby Q_B (*8*, *10*). The second ET is coupled to direct protonation of Q_B (*6*, *8*, *13*−*16*):

[†] This work was supported by grants to P.M. [Hungarian Science Foundation (OTKA T30337), Hungarian Ministry of Education (FKFP 1288, F-29/99, and I-46/99), NSF-OTKA (042-33427), and NATO (LST.CLG 975754)].

* Corresponding author. Phone: 36-62-544-120. Fax: 36-62-544-121. E-mail: pmaroti@physx.u-szeged.hu.

[1] Abbreviations: BIS-TRIS PROPANE, 1,3-bis[[tris(hydroxymethyl)methyl]amino]propane; CAPS, 3-(cyclohexylamino)-1-propanesulfonic acid; CHES, 2-(*N*-cyclohexylamino)ethanesulfonic acid; cyt *c*, cytochrome *c*; EDTA, ethylenediaminetetraacetic acid; ET, electron transfer; LDAO, *N*,*N*′-dimethyldodecylamine *N*-oxide; MES, 2-(*N*-morpholino)ethanesulfonic acid; MOPS, 3-(*N*-morpholino)propanesulfonic acid; P, bacteriochlorophyll dimer; Q_A and Q_B, primary and secondary quinone acceptor; *Rb*., *Rhodobacter*; RC, reaction center; TRIS, tris(hydroxymethyl)aminomethane; Triton X-100, octylphenol polyethylene glycol ether; UQ_6, 2,3-dimethoxy-5-methyl-6-hexaisoprenyl-1,4-benzoquinone; UQ_{10}, 2,3-dimethoxy-5-methyl-6-decaisoprenyl-1,4-benzoquinone.

10.1021/bi0021636 CCC: $20.00
Published on Web 01/17/2001

$$Q_A^- Q_B^- + H^+ \xleftrightarrow{\text{first proton}} Q_A^-(Q_BH) \xrightarrow{\text{second electron}} Q_A(Q_B^-H)^- \quad (3)$$

The uptake of the second proton leads to the formation of quinol:

$$Q_A(Q_BH)^- + H^+ \xrightarrow{\text{second proton}} Q_A(Q_BH_2) \quad (4)$$

The quinol dissociates from the RC and is replaced by an oxidized quinone from the quinone pool:

$$Q_A(Q_BH_2)^- + Q_{pool} \xrightarrow{\text{quinol release + quinone binding}} Q_AQ_B + QH_2 \quad (5)$$

During the quinone reduction cycle, two electrons are transferred and two protons are bound to Q_B. As a result of two coupled photochemical reactions, the RC separates reducing (QH_2) and oxidizing (cyt c^{3+}) equivalents that are exported on the acceptor and donor sides, respectively.

Whereas the pathway, kinetics, and energetics of electron transfer are well documented, those for proton delivery to Q_B are more obscure (*2*, *4*, *16*−*18*). A wide range of structural (*11*, *19*), mutational (*20*−*25*), and computational (*26*, *27*) studies have identified possible proton delivery pathways controlled by several key residues (Asp L210, Glu L212, Asp L213, and Ser L223) in the vicinity of Q_B. Replacement of these crucial amino acids by nonprotonatable amino acids causes severe drop of ET rate and/or proton uptake. The protonation pathways connect the cytoplasmic surface of the RC to these key residues. They consist of a connected network of proton donor and acceptor groups of suitable energetics (pK_a values) linked by hydrogen bonds. Three pathways with different lengths and entry points for the protons were identified (*11*, *13*, *19*).

Very recently, a new method (reversible binding of metal ions to RC) was introduced (*28*, *29*) that has proved to be very successful in identification of the dominant proton delivery pathway to Q_B (*30*). Upon binding of metal ion (Zn^{2+} or Cd^{2+}) to the surface of the RC, at least a 10-fold decrease in the rate of proton transfer was observed that was attributed to severe blockage of the main (P3) proton transfer route to Q_B (*4*, *30*, *31*). On the basis of X-ray diffraction data, the locations of the binding sites for Cd^{2+} and Zn^{2+} were found to be identical and were identified as a cluster of two histidine residues (His H126 and His H128) and one aspartic acid residue (Asp H124) near the surface of the RC on the H subunit at a distance 18 Å away from Q_B (*32*). The Ni^{2+} binds at a nearby location to Asp M17 and His H126 (*33*).

All available reports on inhibition of proton transfer to Q_B by binding of Zn^{2+} or Cd^{2+} transition metal ions have been referred to a single pH (8.0). In this work, we extended the study of the inhibitory effect to a wide pH range and investigated the effect of a more potent transition metal ion, Ni^{2+}; the conventional flash kinetic assays were extended by direct measurement of proton kinetics and stoichiometry attributed to light excitation and metal ion binding to the RC and by assessment of the steady-state turnover rate of the RC. The inhibitory effect was highly pH-sensitive for two reasons: (1) the metal−ligand formation is pH-dependent and (2) the metal binding perturbs the function of the quinone acceptor complex by electrostatic interaction that induces pK_a shifts of the key residues. We address the mechanisms of complexation of metal ions with the RC and electrostatic perturbation of the charged residues by bound metal ions in the quinone complex.

MATERIALS AND METHODS

Electron Acceptors, Electron Donors, Reagents, and Buffers. Ubiquinone UQ_{10} (Sigma) was sonicated in 30% nonionic detergent Triton X-100 (Sigma), and ubiquinone UQ_6 (Sigma) was solubilized in ethanol. Terbutryne (Chem Service, Inc., West Chester, PA), a Q_B site electron transfer inhibitor, was prepared in ethanol before use. A neutral (ferrocene) or charged electron donor [mammalian (horse heart) cytochrome *c* (Sigma)] was used as an external donor to the oxidized dimer (P^+) of the RC in multiple flash experiments (*8*, *34*−*36*). The cytochrome *c* was reduced (>95%) by hydrogen gas on palladium or by sodium ascorbate. The degree of reduction of the cytochrome *c* was monitored by the increase of the optical density at 550 nm in a spectrophotometer (Unicam UV4). The amount of cytochrome *c* oxidized by the RC was determined using the extinction coefficient difference of $\epsilon_{red} - \epsilon_{ox} = 21.1 \pm 0.4$ mM^{-1} cm^{-1} (*37*). Solutions of hydrochloric acid (HCl) were prepared from 10 mM stock solution (Fisher). The following pH indicator dyes were used at the indicated pH ranges at a measuring wavelength close to the isosbestic point of the P/P^+ difference absorption spectrum ($\lambda \approx 570$ nm): bromocresol purple (Reanal) 5.5 < pH < 7.5, *o*-cresol red (Reanal) 7.0 < pH < 9.0, and *o*-cresol−phthalein (Reanal) 8.7 < pH < 10.1. The following pH buffers were used at the indicated pH ranges: MES (Sigma) 5.5 < pH < 6.7, TRIS (Reanal) 7.8 < pH < 8.8, MOPS (Sigma) 6.5 < pH < 7.8, BIS-TRIS PROPANE (Sigma) 6.5 < pH < 9.5, CHES (Sigma) 8.5 < pH < 10.1, and CAPS (Sigma) 9.7 < pH < 11.1.

Transition Metal Ions. For all of the transition metal ions tested in this study, the same anion (Cl^-) was used; thus the difference in the inhibitory effects cannot be attributed to the anionic counterion. The observed effects of the exogenous transition metal ions could be eliminated by addition of a strong chelater of cationic metals (e.g., EDTA).

Isolation and Preparation of the RC. The RC protein was solubilized by the ionic detergent LDAO (Fluka) from the blue-green (carotenoid-less) mutant (strain R-26) of the photosynthetic purple bacterium *Rhodobacter sphaeroides* as described earlier (*8*). For alternate nonionic detergent (Triton X-100, Sigma) preparation and removal of excess salt, the RC preparation was thoroughly dialyzed against 1 mM TRIS buffer (pH 8.0) and 0.03% Triton X-100 overnight at 4 °C before use. Additional extensive dialysis occurred to remove the chelating agent EDTA and, before proton uptake/release measurements, to lower the buffering capacity of the preparation. The RC isolated in this way was depleted of secondary quinone as checked by biexponential analysis of the kinetics of flash-induced charge recombination, where the slow component indicated the presence of functional Q_B (*5*, *38*). The secondary quinone activity was reconstituted by ubiquinones added to the sample in excess from 10 mM stocks. The degree of reconstitution was above 90%.

Electron Transfer Measurements. Charge recombination kinetics were measured by monitoring the recovery of the

oxidized dimer (P^+) at 430 or 865 nm after excitation with a saturating Xe flash of light by using a single-beam spectrophotometer of local design (*8*). The bandwidth of the measuring beam was 2 nm in the visible spectral range and 4 nm at 865 nm. The concentration of the oxidized dimer was determined from the amplitude of the flash-induced absorption change at 430 or 865 nm using extinction coefficients of 26 mM^{-1} cm^{-1} and 120 mM^{-1} cm^{-1}, respectively (*5*, *8*).

The kinetics of the transfer of the first electron from Q_A to Q_B was determined by monitoring the shift of the bacteriopheophytin band at 398 nm. As the reporter bacteriopheophytin is located at different distances from the two quinones, its absorption is sensitive to which of the quinones (Q_A or Q_B) is reduced. To improve the signal-to-noise ratio, routinely 64 traces were averaged.

The kinetics of the proton-coupled second electron transfer from Q_A to Q_B was measured by monitoring the decay of the semiquinone absorption at 450 nm after the second saturating flash in the presence of an external donor (reduced cytochrome *c*).

The kinetics of photooxidation of reduced cytochrome *c* under rectangular shape of laser excitation was measured with a single-beam kinetic spectrophotometer (*39*−*41*). The actinic illumination was provided by a laser diode [HPD, emission wavelength 808 nm, emission bandwidth (fwhm) <3 nm, maximum power 1.0 W] controlled by a homemade driver (operating current 1.2 A). The measuring beam (550 nm) was focused on a small area (3 mm × 3 mm) of the sample. The sample was deoxygenated before measurements and was kept under nitrogen atmosphere.

Proton Binding and Unbinding Measurement. Stoichiometry and kinetics of light-induced proton uptake of the RC were measured by absorption changes of pH indicator dyes (*8*, *42*). Proton release induced by metal ion binding to the dark-adapted RC was measured as the electric response of the pH glass electrode (glass/Ag/AgCl combination semielectrode, Corning No. 476540). Net proton binding/unbinding was obtained by subtraction of the dye or pH electrode response from that measured in buffered (10 mM) solution. External [acid (HCl) mixing] and/or internal (Q_B reconstitution, neutral or acidic pH range) calibrations were carried out. All measurements were performed at room temperature (23 °C).

Data Analysis and Calculations. Experimental data were recorded by a digital oscilloscope (Hitachi VC 6025) interfaced with an IBM PC where data analyses were carried out. The multiexponential decomposition of the absorption transients was performed by using the software package f2 (developed by Z. Filus and G. Laczkó, University of Szeged) based on the Levenberg−Marquardt nonlinear least-squares fitting algorithm. The working models were analyzed numerically by the software package of MathCad 4.0.

RESULTS

pH Dependence of Binding of Transition Metal Ions to the RC. As EDTA in the metal ion−RC complex acts as a chelating agent, it was thoroughly removed before treatment with transition metals. Similarly, as in ref *30*, the observed second electron transfer rate ($k_{AB}^{(2)}$, eq 3) was used to measure the dissociation constant of transition metal ion

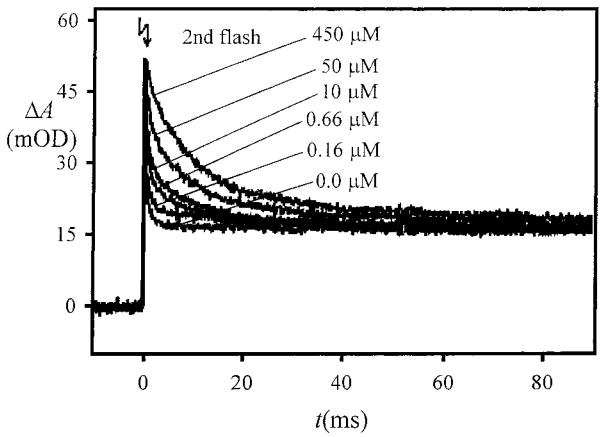

FIGURE 1: Kinetics of the absorption decay of the semiquinones after the second flash (ΔA) measured at 450 nm in the presence of various concentrations of $NiCl_2$. The traces were decomposed into two (slow and fast) phases. The slow and fast components are due to RCs that bind and do not bind Ni^{2+}, respectively. Numerically, $k_{AB}(\text{slow}) = 90\ s^{-1}$ and $k_{AB}(\text{fast}) = 3300\ s^{-1}$. Conditions: 1.5 μM RC, 0.03% Triton X-100, 20 μM cyt c^{2+}, 20 μM UQ_{10}, pH 6.3, 20 mM MES, and $K_D = 30$ μM.

binding to the RC. The rate $k_{AB}^{(2)}$ was determined from the absorption decay curves of the semiquinones after the second saturating flash at 450 nm (Figure 1). The constant (in this time scale not decaying) part of the traces is due to the absorption change of the cytochrome used as the external donor in this experiment. The kinetics slows down with increasing Ni^{2+} concentrations: $k_{AB}^{(2)}$ decreases from an initial value of $k_{AB}^{(2)}(\text{fast}) = 3300\ s^{-1}$ to a limiting value of $k_{AB}^{(2)}(\text{slow}) = 90\ s^{-1}$. The kinetics of the absorption change (ΔA) measured at arbitrary Ni^{2+} concentrations, can be decomposed into two components:

$$\Delta A(t) = A_{\text{fast}} \exp[-k_{AB}^{(2)}(\text{fast})t] + A_{\text{slow}} \exp[-k_{AB}^{(2)}(\text{slow})t] \quad (6)$$

The slow and fast components are attributed to RCs that bind and do not bind Ni^{2+}, respectively. The fraction of the amplitude of the slow phase as a function of Ni^{2+} concentration is described by a standard binding equation that enables the calculation of the dissociation constant (eq A4 in Appendix 1).

Following this procedure at different pH values, the pH dependence of the observed dissociation constant for Ni^{2+} and Cd^{2+} ions was determined (Figure 2.). The lower and upper limits of the pH range were set by the small gap between the limiting (fast and slow) transfer rates that caused uncertainty in biexponential peeling of the kinetic traces (see eq 6). The logarithmic scale indicates a large variation of K_D on pH: the binding affinity of Ni^{2+} decreases by 2 orders of magnitude if the pH is dropped from 8 to 5. A similar but somewhat smaller decrease of binding affinity of Ni^{2+} can be observed on the alkaline pH range (pH >8). The measurements for the Cd^{2+} ion could be performed on a narrower pH range. The K_D of the Cd^{2+} ion shows less pronounced pH dependence, and its binding affinity is larger than that of the Ni^{2+} ion at any pH. It should be noted, however, that the Ni^{2+} is more effective than the Cd^{2+} in inhibition of the second electron transfer: $k_{AB}^{(2)}(\text{slow})$ is 90 s^{-1} for Ni^{2+} and 300 s^{-1} for Cd^{2+} at pH 6.3 (see more details later).

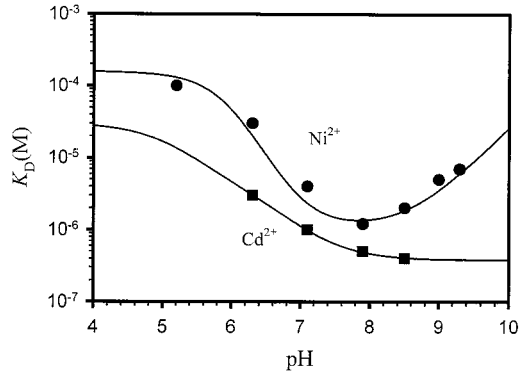

FIGURE 2: pH dependence of the observed dissociation constant of two transition metal ions, Cd^{2+} (■) and Ni^{2+} (●), to RC. The dissociation constants (K_D) were determined from titration of the metal ions (see Figure 1); the kinetics of the second electron transfer was decomposed into two components, and the fraction of the slow phase was adjusted to a simple binding model. Solid lines to the data points were calculated from Scheme 1 using eq A4 in Appendix 1 with the fitting parameters listed in Table 1. Note the increase of the dissociation constant at the acidic pH range. The binding of the metal ions to the RC is tight at the neutral and alkaline pH range.

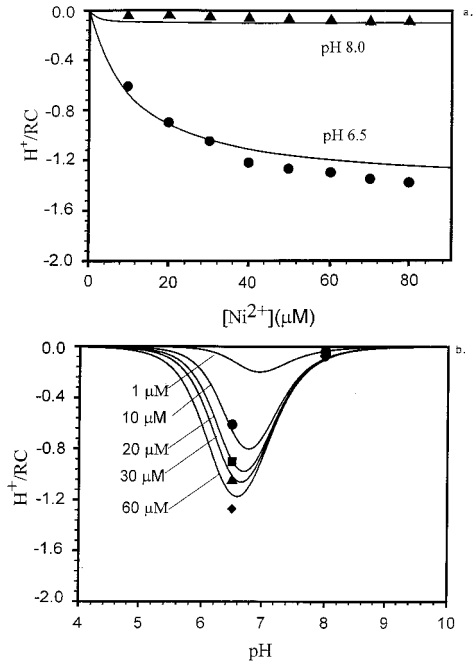

FIGURE 3: Proton release attributed to complexation of Ni^{2+} with the RC. The unbinding of H^+ ions was related to the concentration of the RC upon metal ion titration at two different pH values (a) and upon pH titration at different concentrations of Ni^{2+} (b). The solid curves to the measured data points were calculated from the working model (Scheme 1) using eq A14 in Appendix 1 with the pK_a and K_D values given in Table 1. Conditions: 1.5 μM RC, 0.03% Triton X-100, and 50 mM NaCl.

Measurement of Proton Release Due to Metal Ion Binding. The marked pH dependence of the dissociation constant of transition metal ion binding to the RC shows the involvement of protons in the binding process. The proton release associated with Ni^{2+} ion binding to the RC was directly measured by the pH glass electrode after addition of the metal ion in buffer-free solution of the RC (Figure 3). The stoichiometry of proton unbinding was determined by mixing of acid (HCl) of calibrated concentration. The solution had a high ionic strength (50 mM) to obtain a stable and well-defined pH change upon addition of Ni^{2+} ion. Depending on the pH and buffering capacity of the solution, a pH drop was observed. The acidification of the solution may be explained by proton release upon binding of Ni^{2+} to the RC and/or by decreased activity of OH^- ions by binding to cationic Ni^{2+}. The latter is a bulk effect, and its extent should depend linearly on the Ni^{2+} concentration. The Ni^{2+} titration curve of the RC solution showed saturation in the expected range of the Ni^{2+} concentration and did not perform monotonically increasing tendency as could be predicted in the case of the bulk effect of the Ni^{2+} ion (Figure 3a). This is a strong argument in favor of proton release due to Ni^{2+} binding to the RC. The bulk effect of added Ni^{2+} must be subtracted to obtain the true proton release. The proton release showed strong pH dependence and was restricted to a relatively small pH range (Figure 3b). At (or close to) saturating Ni^{2+} concentration (≈100 μM), the RC can unbind 1.5 H^+ ions at pH 6.5, whereas at pH 8.0, the proton release is about 10 times smaller.

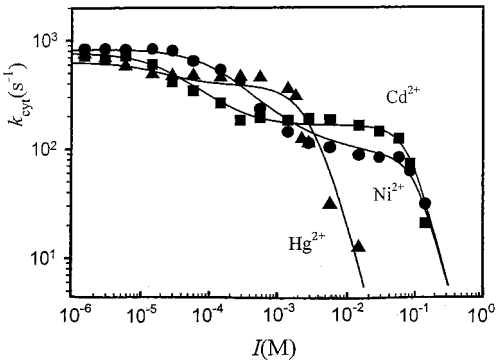

FIGURE 4: Inhibitory effect of transition metal ions Cd^{2+} (■), Ni^{2+} (●), and Hg^{2+} (▲) on the rate of steady-state turnover of the RC, measured as the rate of cytochrome photooxidation, k_{cyt}, vs ionic strength (I) of the bivalent metal ion. The inhibition occurs in two waves: retardation of the proton transfer by binding of the bivalent ions (observed at low ionic strengths) and ionic screening of the RC and cyt c^{2+} or direct interaction with surface charged groups (at high ionic strengths). Solid lines are the best fit of eq A21 in Appendix 2 (Scheme 2) with $k_{off}(I\rightarrow\infty) = 1 \times 10^6$ s^{-1}, $k_{AB}^{(2)}$ (not inhibited, pH = 6.0) = 6000 s^{-1}, and $k_I = 4500$ s^{-1} (for all metal ions) and the other parameters as listed in Table 3. Conditions: 1.0 μM RC, 0.03% Triton X-100, 58 μM cyt c^{2+}, 25 μM UQ_6, and pH 6.0.

Inhibition of the Cytochrome Turnover. The transition metal ions bound to the surface of the RC inhibit both the first (*28*) and second electron transfer processes (*30*, *31*). We demonstrate that not only the rates of the individual electron transfer steps but also that of the overall continuous turnover of the protein are slowed due to binding of transition metal ions to the RC. The steady-state turnover rate of the RC was measured by detection of the rate of photooxidation of cytochrome under rectangular shape of excitation by a laser diode (*39*, *40*). For a variety of mono-, di-, and trivalent cations, the general tendency of the ion titration curves was already established (*41*): the rate was retarded at low ionic strength and accelerated as the salt concentration was increased. At the maximum (e.g., for NaCl at 40 mM), the rate was 2−3 times higher than at limiting low ionic strength. At still higher salt concentrations, the rate of photooxidation of the cytochrome declined sharply. The titration curves of the transition metal ions, however, deviate from this general behavior (Figure 4). The deviation is more pronounced at

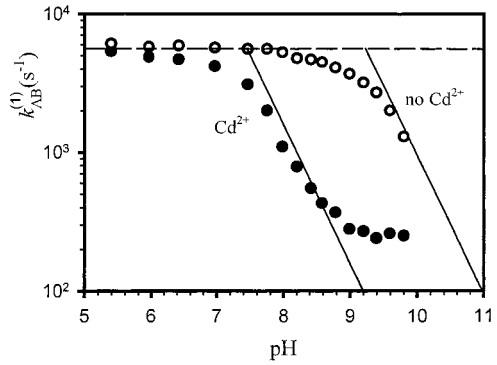

FIGURE 5: Effect of Cd^{2+} on the rate of proton-coupled first electron transfer ($k_{AB}^{(1)}$) as a function of pH. The apparent pK_a value (9.2) attributed to protonation of Q_B coupled (cluster of) amino acid(s) in the absence of Cd^{2+} (○) is shifted to lower pH by about 1.8 pH units in the presence of Cd^{2+} (●). The kinetics was measured at 398 nm, was the average of 64 traces, and was decomposed into a single exponential function. Conditions: 2.5 μM RC, 0.03% Triton X-100, 20 μM UQ_{10}, and 100 μM Cd^{2+}.

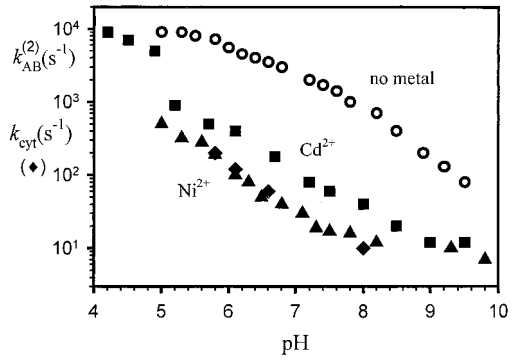

FIGURE 6: Decelerating effect of Cd^{2+} (■) and Ni^{2+} (▲) transition metal ions on the rate of proton-coupled second electron transfer [$k_{AB}^{(2)}$, (○) for no metal ions] and steady-state cytochrome turnover in the Ni^{2+}-inhibited RC (◆) as a function of pH. The rate of continuous turnover of the RC is limited by $k_{AB}^{(2)}$ in the presence of Ni^{2+}. Conditions: 1.5 μM RC, 0.03% Triton X-100, 20 μM cyt c^{2+}, 20 μM UQ_{10}, 100 μM Cd^{2+} (■), and 800 μM Ni^{2+} (▲ and ◆).

low ionic strength: not an increase but a decrease can be observed that turns into the overall drop at high ionic strength. The Cd^{2+} and Ni^{2+} ions act similarly, but the behavior of the Hg^{2+} ion is different: the rate is nearly constant at low ionic strength, and the sharp drop starts at significantly lower ionic strength (≈2 mM).

pH Dependence of Electron and Proton Transfer of the Inhibited RC. Different photochemical assays were used to investigate the changes in electron and proton transfer properties of the RC upon binding of transition metal ions. At all pH values in these experiments, the concentration of the transition metal ion was high enough to saturate the binding site of the RC.

Figure 5 shows the pH dependence of the observed rates of the first electron transfer to Q_B ($k_{AB}^{(1)}$, eq 2) in untreated and inhibited RCs. At neutral and acidic pH range, only slight deceleration of the transfer could be observed in the presence of Cd^{2+} ions. The reduction of the rate, however, increased progressively upon pH increase in the alkaline pH range. In good accordance with earlier results (*30*), the rate was reduced ≈10-fold at pH 8.0 and stabilized at a low (residual) level of ≈200 s^{-1} at pH 10. By fitting straight lines of slope −1 to the pH-dependent parts of the measured curves, $k_{AB}^{(1)}$ of the Cd^{2+}-treated RC can be derived from that of the untreated RC by a 1.8−2.0 pH unit shift toward the acidic pH range.

A similar tendency was observed in the pH dependence of the second electron transfer rate ($k_{AB}^{(2)}$, eq 3 and Figure 6). At low pH (<5.0), only a small difference can be seen between the rates of treated and untreated RCs. Although the transition metal ions are bound to the RC (see Figure 2), they do not inhibit the rate of proton-assisted electron transfer significantly. The difference between the rates in the absence and presence of transition metal ions is large on a wide pH range (5.0 < pH < 8.5) but seems to disappear again at high pH values. The Cd^{2+} ion is somewhat less effective than the Ni^{2+} ion. The steady-state turnover rate of the cytochrome in the RC inhibited by the Ni^{2+} ion coincided with the rate of the second electron transfer. This indicates that the binding of Ni^{2+} to the RC decreased $k_{AB}^{(2)}$ so enormously (about 2 orders of magnitude) that it became the slowest step in the quinone reduction cycle (pH > 5).

The pH profile of $k_{AB}^{(2)}$ is more difficult than that of $k_{AB}^{(1)}$ (see Figure 5) as the reaction goes through a protonated semiquinone intermediate (eq 3 and ref *43*) and is coupled to the protonation states of several (cluster of) ionizable amino acids. The pH dependence of $k_{AB}^{(2)}$ cannot be characterized by a single slope. Upon increase of the pH, the pH dependence becomes progressively more pronounced, and the slope approaches −1.0 in the alkaline pH values. In good accordance with earlier results, we found that the pH dependence of the native RC did not differ very much from that of the inhibited sample (*30*). Formally, the same values of $k_{AB}^{(2)}$ are observed in Cd^{2+}- (and Ni^{2+}-) treated and native RCs if the pH values of the untreated sample are shifted by about 2.0 (and 2.5) units to the acidic pH range.

To study further the modified function of protonatable groups in the inhibited RC, the stoichiometry and kinetics of flash-induced proton uptake were measured in different states of the RC. Figure 7 shows the pH dependence of proton binding upon transitions of $PQ_A \rightarrow P^+Q_A^-$ (a) and $PQ_B \rightarrow P^+Q_B^-$ (b) in the native and inhibited RC. In contrast to the very significant drop of rates of electron transfer kinetics described above, the binding of the transition metal ion to the RC causes only small changes in the stoichiometry of the light-induced proton uptake. A slight increase below pH 9 (about 0.1 H^+/RC and 0.2−0.3 H^+/RC for Q_B inactive and Q_B active RCs, respectively) and similar size of drop above pH 9.0 can be seen upon transition metal ion treatment. The change is even smaller if only the acceptor quinone undertakes redox transition: $Q_B \rightarrow Q_B^-$ [an external electron donor (ferrocene) is applied to rereduce the oxidized dimer] (Figure 7b). Formally, the pH profiles of native and inhibited RCs overlap upon a pH shift of about 1.5 units.

Addition of exogenous Cd^{2+} causes a significant decrease in the observed rates of proton binding after the first ($k_H^{(1)}$, Figure 8a) and second ($k_H^{(2)}$, Figure 8b) flash between pH 7 and pH 10. In the inhibited RC, the measured rates of proton uptake are the same as the transfer rates of the first ($k_{AB}^{(1)}$, Figure 8a) and second ($k_{AB}^{(2)}$, Figure 8b) electron to Q_B. The complex formation of the transition metal ion and RC reduces the binding rates of the first and second proton, and the uptake of H^+ ions will limit the corresponding electron transfer steps on lower rates.

The inhibitory effect of the transition metal ions can be

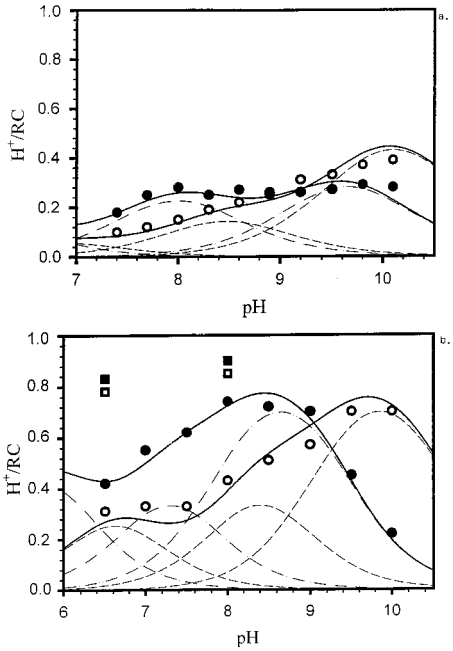

FIGURE 7: pH dependence of proton binding stoichiometry due to different flash-induced transitions of the RC in the absence (○, □) and in the presence of 100 μM Cd^{2+} (●, ■). (a) $PQ_A \rightarrow P^+Q_A^-$: solid lines are best fits of Henderson−Hasselbalch curves (*8*) for three protonatable noninteracting residues with the dark/light (PQ_A/$P^+Q_A^-$) pK_a values listed in Table 2; dashed lines are individual contributions of the residues. (b) $PQ_B \rightarrow P^+Q_B^-$ (○ and ●): solid lines are best fits of Henderson−Hasselbalch curves (*8*) for three protonatable noninteracting residues with the dark/light (PQ_B/$P^+Q_B^-$) pK_a values listed in Table 2; dashed lines are individual contributions of the residues. $PQ_B \rightarrow PQ_B^-$ (□ and ■): external donor (200 μM ferrocene) rereduced P^+ after flash excitation and the proton uptake of secondary semiquinone could be determined. The proton binding was corrected for not complete secondary quinone activity. Conditions: 1.5 μM RC, 0.03% Triton X-100, 50 mM NaCl, 40 μM pH indicator dye, ±10 mM buffer (depending on pH, see Materials and Methods for details), 100 μM terbutryne (a), and 40 μM UQ_{10} (b).

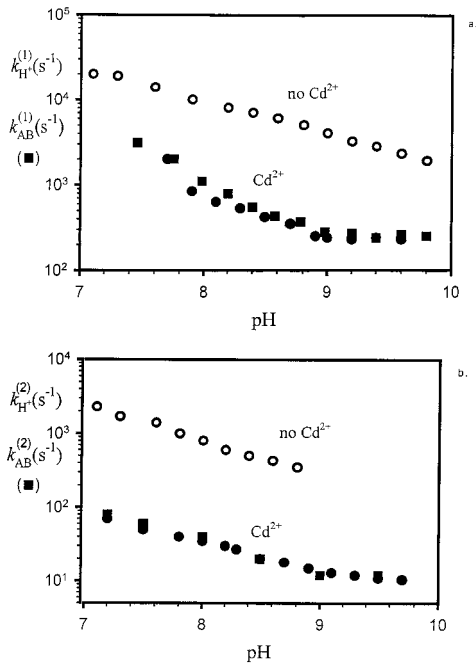

FIGURE 8: pH dependence of the rates of light-induced proton binding (k_H) after the first (a) and second flashes (b) in the absence (○) and presence (●) of 100 μM Cd^{2+} together with rates of first [$k_{AB}^{(1)}$, (a) ■] and second [$k_{AB}^{(2)}$, (b) ■] interquinone electron transfer in the inhibited RC. The kinetics was followed by absorption changes of the pH indicator dyes *o*-cresol red and *o*-cresol−phthalein (depending on pH) at 586 nm. Conditions: 2.0 μM RC, 30 μM pH indicator dye, ±10 mM buffer, 100 μM Cd^{2+}, 0.03% Triton X-100, 50 mM NaCl, 100 μM terbutryne (a), average of 64 traces (a), and 20 μM UQ_{10} (b), 200 μM ferrocene (b), and 500 μM potassium ferrocyanide (b).

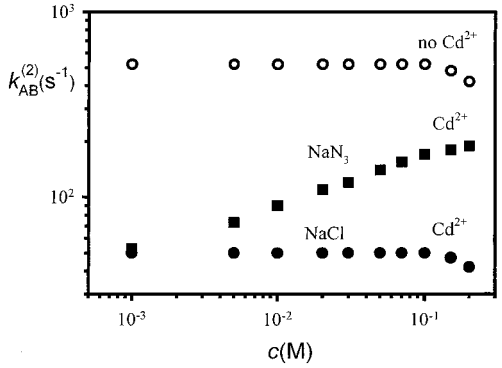

FIGURE 9: Accelerating effect of azides on proton transfer rate in the RC inhibited by bivalent transition metal ion (100 μM Cd^{2+}). Second electron transfer rate ($k_{AB}^{(2)}$) vs concentration of sodium azide [NaN_3, with (■) and without (○) Cd^{2+}] and sodium chloride [NaCl, (●)] as reference. Conditions: pH 8.0, 1.5 μM RC, 20 μM cyt c^{2+}, 20 μM UQ_{10}, 20 mM TRIS, and 0.03% Triton X-100.

partly reduced by addition of exogenous sodium azide (NaN_3). Figure 9 demonstrates this accelerating effect as a function of azide concentration. The 10-fold decrease of $k_{AB}^{(2)}$ due to Cd^{2+} binding is gradually lowered to a factor of only 2 at high (200 mM) azide concentration. A similar titration experiment with NaCl as reference had no effect. The observed partial recovery of the electron and proton transfer kinetics is not due to modification of the Cd^{2+}−RC complex by the azide. The dissociation constant of Cd^{2+} was determined in the absence and in the presence of 20 mM azide (Figure 10). Using the standard binding equation (eq A4 in Appendix 1), the same dissociation constants (K_D = 0.5 μM) were determined in both cases within the error of the experiment. Therefore, the azide does not modify the binding affinity of the transition metal ion to the RC.

DISCUSSION

This work offers experimental evidence for the pH dependence of ligand formation of transition metal ions with the RC and for the pH-dependent nature of the inhibition of several proton-assisted reactions by bound metal ions. An essential aspect of this work is to reveal the importance of electrostatic interaction between the bound metal ion and the key protonatable residues that control the proton transfer from the cytoplasmic phase to Q_B. The discussion will provide an interpretation of how the different proton and electron transfer reactions could be changed upon binding of transition metal ions to the RC.

Complexation of Transition Metal Ions in the RC. The very recent X-ray crystallographic investigations exposed the different coordination spheres around the bound Cd^{2+}, Zn^{2+}, and Ni^{2+} ions in the RC from *Rb. sphaeroides* at pH 8.0 (*32*, *33*). The three water oxygen atoms and one carboxyl (Asp H128) oxygen atom and the two imidazole (His H124 and H126) nitrogen atoms form an octahedron around the cadmium (and the zinc) ion. The two water oxygen atoms

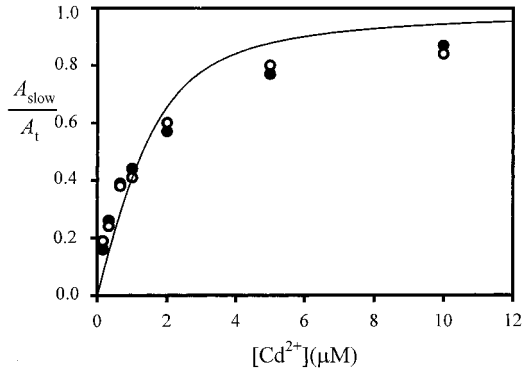

FIGURE 10: Fraction of the slow phase (A_{slow}/A_t) of the second electron transfer kinetics as a function of added $CdCl_2$ concentration in the presence (●) and absence (○) of 20 mM azide. The solid curve is the best fit to the binding equation (A4, Appendix 1) with a dissociation constant of $K_D = 0.5$ μM. Conditions: same as in Figure 9.

and the one carboxyl (Asp M17) oxygen atom with the nitrogen atom from the imidazole ring of His H124 form a tetrahedron around the Ni^{2+} ion. However, no structural data are available for different pH values. Thermodynamic equilibrium studies were carried out to investigate the mechanism of pH regulation of binding affinity based on direct determination of the dissociation constant (Figure 2).

The molecular basis for the linkage between ligand affinity and pH stems from alteration of pK_a values of ionizable amino acid groups concomitant with binding. The coordination bonds between His and Asp side chains and the Cd^{2+} (and Ni^{2+}) ion become less stable and finally split upon decrease of pH where the residues become protonated. This behavior is manifested by a significant increase of the dissociation constant in the acidic pH range (Figure 2). A working model is introduced where the metal ions (M: Cd^{2+} or Ni^{2+}) and the H^+ ions compete for complexation with the Asp−His ligand, and additionally M can bind also to the OH^- ions. Scheme 1 depicts a thermodynamic cycle that links ligand binding reactions to perturbation of the ligand-bound and unbound states of the RC by protons. The different ligand binding reactions of the complex can be described by different dissociation constants, and the observed dissociation constant is the pH-dependent combination of these dissociation constants (eq A13 in Appendix 1). The model fits to the measured pH dependence of the dissociation constant with parameters listed in Table 1.

An important consequence of this model is the release of H^+ ions upon complexation under appropriate conditions. We could measure the proton release upon titration of transition metal ions at different pH values (Figure 3). The observed values are in good agreement with the stoichiometry protons linked to the ligand binding reaction and calculated from the working model (see Scheme 1 and Appendix 1). The derivative linkage relationship indicates that the number of protons associated with complexation is equal to the slope of the dissociation constant versus pH (ref *44* and eq A15 in Appendix 1). Indeed, the largest amount of liberated protons is observed between pH 6.0 and pH 7.0 where the pH dependence of the dissociation constant is most pronounced (Figure 2).

Considering the binding affinity, the Asp and His residues in the Cd^{2+} and Ni^{2+} binding sites may have different

Scheme 1: Working Model for Formation of a Metal−Ligand Complex as a Function of pH and Metal Ion (M^{2+}) Concentration[a]

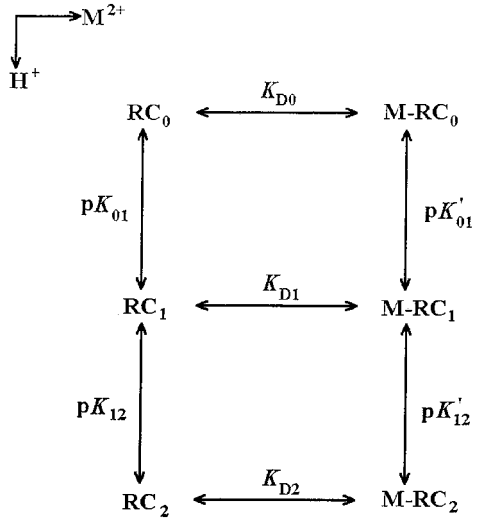

[a] The RC (as ligand) may exist in different protonation states (with 2, 1, and 0 bound protons) depending on the actual pH (vertical direction) and in complex with the metal ion depending on the concentration of the metal ion (horizontal direction). The metal ion may bind to the RC or to the OH^- ion in the solution. The equilibrium constants of the protonation of the different states of the RC (pK_a values), the metal binding (K_D, dissociation constant), and the formation of M−OH (K_{M-OH}) are derived from the best fit analysis of the pH dependence of the dissociation constant (see Figure 2) and are listed in Table 1.

Table 1: Dissociation Constants for Transition Metal Ion Binding (K_D) and Proton Uptake (K_a and K'_a) Associated with the Metal−Ligand Complex in the RC and for Metal OH^- Binding (K_{M-OH}) Described by Scheme 1[a]

transition metal ion	K_{D0} (μM)	K_{D1} (μM)	K_{D2} (μM)	pK_{01}	pK_{12}	pK'_{01}	pK'_{12}	pK_{M-OH}
Cd^{2+}	0.38	3.8	30.2	7.4	5.9	6.4	5.0	ND[b]
Ni^{2+}	1.0	12.6	159	7.0	7.0	5.9	5.9	5.4

[a] These values were determined from the best fit to experimental data in Figure 2. [b]ND, not determined.

significance. Very recently, a double mutant was constructed in which the two histidines (His H126 and His H128) were replaced with alanines (*44*). In the stoichiometric concentration range of the metal ions, no significant decrease in $k_{AB}^{(2)}$ was observed in the double mutant compared to the native RC. However, addition of metal ions in high concentration (>1 mM) could decrease $k_{AB}^{(2)}$, showing significantly decreased binding affinity for Cd^{2+} and Ni^{2+} in the histidine mutant. The pH dependence of our binding studies signified that the largest changes in the dissociation constant occurred in the pH range where the protonation of the histidines can be expected (Figure 2). These results lead to the conclusion that histidines play a key role in complexation of these transition metal ions to the RC as binding of Cd^{2+} and Ni^{2+} to the histidine residues is significantly stronger than to the aspartic acid residues.

Kinetic Correlation between Electron and Proton Transfers in the Inhibited RC. Upon binding of transition metal ions, both electron transfer (as measured by $k_{AB}^{(1)}$, $k_{AB}^{(2)}$, and k_{cyt}) and flash-induced proton uptake (as measured by k_H) became slow and kinetically correlated. Considering the transfer of the first electron, we argue that the decrease in

Scheme 2: Simplified Kinetic Scheme of Dominating Electron Transfer Reactions for Calculation of the Observed Rate of Steady-State Turnover of the RC[a]

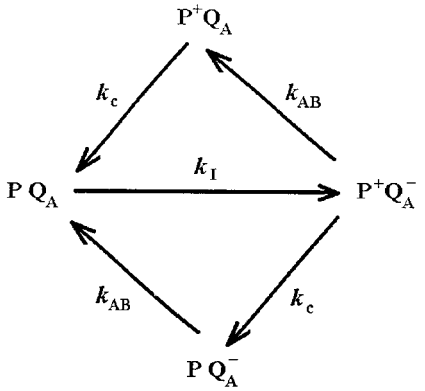

[a] Continuous illumination leads to charge separation ($PQ_A \rightarrow P^+Q_A^-$) with rate constant k_I. The charges disappear by rereduction of P^+ by reduced cytochrome *c* ($P^+Q_A^- \rightarrow PQ_A^-$ or $P^+Q_A \rightarrow PQ_A$, rate constant k_c) and by reoxidizing Q_A^- by Q_B or Q_B^- ($P^+Q_A^- \rightarrow P^+Q_A$ or $PQ_A^- \rightarrow PQ_A$, effective rate constant k_{AB}).

the rate is attributed to the reduction of the rate of the conformationally gated step (eq 2, ref *7*). The conformational gating is controlled by a complex interaction of protein and proton rearrangements (*3*, *26*, *27*). The flash-induced uptake and redistribution of protons stabilize the semiquinone, and these processes are kinetically severely hindered by binding of transition metal ions. The observed kinetic correlation between $k_{AB}^{(1)}$ and $k_H^{(1)}$ in the inhibited RC indicates that the proton rearrangement slows down and becomes rate limiting in the transfer of the first electron.

Similar kinetic coupling was observed between the transfer of the first proton and second electron to Q_B occurring with rate constant $k_{AB}^{(2)}$ (see eq 3). As observed earlier (*30*), the transfer of the first proton becomes rate limiting in the presence of transition metal ions (Figure 8b). To reveal the possible effect of transition metal ions on rates of further steps (see eqs 4 and 5), steady-state turnover measurements were carried out. The decrease of the rate of the cytochrome photooxidation upon increasing concentration of the transition metal ions could be described by a simple model taking into account the direct effect of metal binding and ionic screening of the interacting proteins (Scheme 2 and Appendix 2). The rate of turnover followed the rate of proton-assisted second electron transfer (Figure 6). As $k_{AB}^{(2)}$ remained the smallest rate in the quinone reduction cycle of the inhibited RC, the uptake of the second proton (eq 4) must remain rapid and less perturbed by transition ions than the uptake of the first proton.

The similar behavior of the different electron and proton transfer kinetics upon binding of transition metal ions calls for a common mechanism, which we can signify as electrostatic perturbation of uptake and/or rearrangement of protons after light excitation.

pK_a Changes of Key Protonatable Groups Due to Bound Metal Ion. Several indirect effects of bound transition metal ions can lead to the observed inhibition of proton transfer in the RC: changes in proton donation properties of the Asp and His residues participating in ligand formation, steric hindrance, and modification of dynamics and functional organization of the proton channels connecting the bulk phase to the Q_B site. Not neglecting the importance of these possible effects, our results strongly suggest that the direct effect of electrostatic repulsion of protons by the bound metal ion could be the major contribution.

The electrostatic interaction with the cationic metal ion induces pK_a shifts of nearby amino acids that control the proton transfer to Q_B. Assuming elementary charges on the metal ion and the ionized residue at a distance of 10 Å and a dielectric constant of 15, the interaction energy is estimated to be 100 meV. (For discussion of the choice of the dielectric constant, see refs *43* and *46*.) This interaction energy lowers the pK_a of the protonatable residue by 1.6 units. The pK_a shifts observed in our experiments were in the same range. Here, we refer only to the pH dependence of the stoichiometry of the flash-induced proton uptake where the pK_a values were (down) shifted by similar magnitudes in both the dark and light states of the RC due to electrostatic interaction with the bound metal ion (see Figure 7 and Table 2). This gradual shift did not cause significant alteration in binding stoichiometry.

The identification of these residues is not yet straightforward, and our methods have only limited access to the answer. The pH dependence of proton uptake and electron transfer rates indicates the contribution of several groups in key positions. They are arranged in clusters with possibly complex titration behavior that makes it difficult to attribute the observed pK_a values to any one amino acid (Figure 7 and Table 2). It was demonstrated that Glu L212 and Asp L213 showed nonclassic titration behavior due to strong electrostatic interaction (*47*, *48*). Reasonable candidates for key residues are Ser L223, Asp L213, Asp L210, Asp M17, Glu L212, and Glu H173. Using calculations of side chain ionization and conformation, the pH dependence of the proton uptake was interpreted by the assumption of Asp L210 as the internal proton donor to the key residues (Ser L223, Asp L213, and Glu L212) closer to Q_B (*26*). Recent mutational studies demonstrated the important role of Asp L210 in the proton transport (*31*). We believe that the bound metal ion lowers the pK_a values of these residues and results in acidic pH shifts in electron and proton transfer properties compared to those of the native RC. This could be the reason the effect of metal binding diminished significantly at low and high pH values. In these pH ranges, the pK_a shift due to bound metal ion could not cause marked alteration in ionization properties of the key protonatable residues.

In accordance with recent observations by Paddock et al. (*30*), the kinetics (rates and amplitudes) of the $P^+Q_B^- \rightarrow PQ_B$ charge recombination remained unchanged upon addition of the transition metal ions over a very broad pH range (data not shown). As the rate of the back-reaction is usually considered as a probe of the local electrostatic environment of the secondary quinone, one can wonder why the electrostatic influence of the metal center does propagate to the acidic cluster only and terminates at Q_B. Several arguments can be mentioned. According to X-ray diffraction data, the metal ion binding site is located ≈20 Å from the Q_B site (*32*) that is too large for significant electrostatic interaction. Long-distance coupling was observed between Q_A^- and Glu L212 in the two quinone binding pockets, but the distance was smaller and the intervening protein matrix was more hydrophobic (the dielectric constant was lower) (*23*, *24*). The key acidic residues interacting with the bound metal ion should locate between the metal binding site and Q_B and

Table 2: Low pH Shift of Dark (RC in PQ_A and PQ_B Redox States) and Light (RC in $P^+Q_A^-$ and $P^+Q_B^-$ Redox States) pK_a Values for Three Noninteracting Protonatable Residues upon Cd^{2+} Ion Binding to the RC[a]

protonatable residues	PQ_A	$PQ_A + Cd^{2+}$	$P^+Q_A^-$	$P^+Q_A^- + Cd^{2+}$	PQ_B	$PQ_B + Cd^{2+}$	$P^+Q_B^-$	$P^+Q_B^- + Cd^{2+}$
1	9.7	9.4	10.5	9.9	9.1	7.9	10.6	9.4
2	8.35	7.8	8.6	8.2	8.1	7.0	8.7	7.6
3	6.8	5.8	6.9	6.1	6.4	5.3	6.85	6.1

[a] The values were obtained from fitting of Henderson−Hasselbalch curves (*8*) to pH dependence of proton uptake in Figure 7.

Table 3: Fitting Parameters of Equation A21 in Appendix 2 That Describe the Ionic Strength Dependence of the Rate Constant of Steady-State Turnover of the RC (Figure 4)

transition metal ion	$k_{on}(I\rightarrow 0)$ (s^{-1})	$k_{on}(I\rightarrow\infty)$ (s^{-1})	$k_{off}(I\rightarrow 0)$ (s^{-1})	R_{RC} (nm)	R_{cyt} (nm)	$k_{AB}^{(2)}(i)$ (s^{-1}) (pH = 6.0)	K_D (μM)
Ni^{2+}	3.8×10^9	1000	1080	0.51	0.23	90	50
Cd^{2+}	3.8×10^9	1000	990	0.51	0.23	170	10
Hg^{2+}	5.0×10^8	100	850	1.61	0.43	560	5

are able to screen the electrostatic influence of the metal ion to charged groups outside this region. Even if some free energy change of Q_B^- ($-\Delta G°$) occurs due to the interaction with the metal complex, it is not sure that it will be reflected as a significant change of the rate of the charge recombination. According to the Marcus theory of electron transfer, a small change in the driving force can be compensated by a small change in the reorganization energy (λ). Upon metal ion binding at the surface of the protein, slight rearrangement of the charged groups can be expected that perturbs the reorganization energy of the electron transfer in the charge recombination process.

Independently of the identification of the key residues that control the pH profile of the transfers, this interpretation needs reconsideration of the concept of the dominant pathway of proton transfer based on metal ion binding studies (*4*, *30*). We argue that all proton delivery pathways that run through the key residues under electrostatic influence of the metal ion are exposed to the inhibitory effect of the transition metal. On the basis of structural data, several proton channels with different proton entry points may be identified (*11*), and these pathways funnel the H^+ ion to the network of key protonatable residues in the vicinity of Q_B. Because these groups are under the electrostatic control of the bound transition metal ion, deceleration of the observed proton transport can be expected independently of which of the channels delivers the proton to the secondary quinone.

Reactivation Effect of Azide. It is a remarkable finding that azide could "reactivate" RC that had highly impaired electron and proton transfer reactions due to treatment with transition metal ions. Originally, this agent was considered to act as an intraprotein proton carrier overcoming dynamic obstacles in the impaired protein (*49*, *50*). Later, mainly on the basis of the very substantial inhibition effect of the mutational lesion at Glu H173, this concept was reconsidered (*51*). The significance of changes in the electrostatics of the protein due to the small acid was recognized (*47*). Both effects of azide may contribute to accelerate the inhibited proton transfer.

The azide helps to adjust the functional pK_a values of the actual proton carriers by electrostatic influence. It probably tries to compensate for the loss of negative potential due to complex formation of the bivalent transition metal ion. This action would correspond to the expectations derived from classical enzymology. The bacterial RC would serve also in this respect as an appropriate model for general proton transfer, but additional studies are required to map the electrostatics of the metal−RC complex.

On the basis of competitive binding studies between azide and RC for metal binding, the trivial effect of the azide to accelerate the proton transfer by removal of the metal ion can be excluded: identical dissociation constants for the Cd^{2+} ion were measured in the absence and presence of azides (Figure 10). Because of the electrostatic nature of binding of the transition metal ion to the RC, the binding affinity is sensitive to the local electrostatics at the binding site. As no modification of the dissociation constant is observed, the electrostatic perturbation of the azide should not be significant. Therefore, the azide can get around the block as an intraprotein proton carrier and can form a proton transporting web similarly as water molecules may create proton conducting channels.

ACKNOWLEDGMENT

We are indebted to Drs. L. Kálmán and G. Laczkó for valuable discussions and careful reading of the manuscript.

APPENDIX

(1) pH Regulation of Binding Affinity of the Transition Metal Ion to the Ligand RC

(1a) Dissociation Constant of Metal Binding to the RC of the Single State. The goal is to find a correlation between the fraction of the slow phase amplitude of the second electron transfer kinetics and the dissociation constant (K_D) of metal ion binding to the RC as the ligand. The added metal ion (M) and RC (subscript t) in the solution can exist in free (subscript f) and bound (M−RC) forms:

$$[M]_t = [M]_f + [M{-}RC] \quad \text{(A1)}$$

$$[RC]_t = [RC]_f + [M{-}RC] \quad \text{(A2)}$$

The dissociation constant is defined by

$$K_D = \frac{[RC]_f[M]_f}{[M{-}RC]} \quad \text{(A3)}$$

As [M−RC] is proportional to the amplitude of the slow

phase (A_{slow}) and $[RC]_t$ to the total amplitude ($A_t = A_{slow} + A_{fast}$), their ratio can be expressed from eqs A1−A3:

$$\frac{A_{slow}}{A_t} = \frac{[M]_t + [RC]_t + K_D - \sqrt{([M]_t + [RC]_t + K_D)^2 - 4[RC]_t[M]_t}}{2[RC]_t} \quad \text{(A4)}$$

(1b) Dissociation Constant of Metal Binding to the RC of Multiple Protonation States. To determine the observed K_D at any pH, we use Scheme 1 with six different states of the RC. The proton dissociation constants are

$$K_{01} = \frac{[RC_0][H^+]}{[RC_1]} \quad \text{(A5)}$$

$$K_{12} = \frac{[RC_1][H^+]}{[RC_2]} \quad \text{(A6)}$$

$$K'_{01} = \frac{[M{-}RC_0][H^+]}{[M{-}RC_1]} \quad \text{(A7)}$$

$$K'_{12} = \frac{[M{-}RC_1][H^+]}{[M{-}RC_2]} \quad \text{(A8)}$$

The dissociation constant of metal−ligand binding at very high pH is

$$K_{D0} = \frac{[RC_0][M]_f}{[M{-}RC_0]} \quad \text{(A9)}$$

The RC exists in six (free and ligated) states:

$$[RC]_t = [RC_0] + [RC_1] + [RC_2] + [M{-}RC_0] + [M{-}RC_1] + [M{-}RC_2] \quad \text{(A10)}$$

The cationic metal ion is either free in the solution or bound to the RC or to OH^- groups (this contribution may be significant at high pH):

$$[M]_t = [M]_f + [M{-}RC_0] + [M{-}RC_1] + [M{-}RC_2] + \frac{[M]_f[OH^-]}{K_{M-OH}} \quad \text{(A11)}$$

The equilibrium of the $M + OH^- \leftrightarrow M{-}OH$ reaction (omitted in eq A1) is described by dissociation constant K_{M-OH}.

The dissociation constant of the metal binding to the RC at any pH is

$$K_D = ([RC_0] + [RC_1] + [RC_2])([M]_t - ([M{-}RC_0] + [M{-}RC_1] + [M{-}RC_2]))/([M{-}RC_0] + [M{-}RC_1] + [M{-}RC_2]) \quad \text{(A12)}$$

Replacing the different ligand concentrations from eqs A5−A11 into eq 12 and taking $[OH^-]$ from the ion product of water, $K_w = [H^+][OH^-] = 1 \times 10^{-14}$, the pH dependence of the observed dissociation constant can be expressed as

$$K_D = K_{D0}\frac{(1 + 10^{pK_{01}-pH} + 10^{pK_{01}+pK_{12}-2pH})(1 + 10^{pK_{M-OH}+pH-14})}{1 + 10^{pK'_{01}-pH} + 10^{pK'_{01}+pK'_{12}-2pH}} \quad \text{(A13)}$$

(2a) Metal Ion Titration of Proton Release Due to Complexation. The stoichiometry of change of protons due to metal binding to the RC is

$$[H^+]/[RC]_t = (([M{-}RC_1] + [RC_1] + 2([M{-}RC_2] + [RC_2])) - ([RC_1]_{M=0} + 2[RC_2]_{M=0}))/[RC]_t \quad \text{(A14)}$$

The concentrations of species in eq A14 can be expressed from eqs A5−A11. The stoichiometry of proton release as a function of added metal concentration, $[M]_t$, is numerically calculated in Figure 3a.

(2b) pH Dependence of Proton Release. Equation A14 can be used also for numeric calculation of proton unbinding as a function of pH. Figure 3b demonstrates typical pH patterns for different metal ion concentrations. The proton stoichiometry can be related directly to the pH dependence of the dissociation constant (see also ref *44*):

$$\frac{[H^+]}{[RC]_t} = \frac{d(\log K_D)}{d(pH)} \quad \text{(A15)}$$

The negative slope of K_D versus pH means proton release as observed in our experiments (Figure 2).

(2) Ionic Strength Dependence of the Steady-State Turnover of the RC Inhibited by Binding of the Transition Metal Ion

The rate constant of cytochrome photooxidation, k_{cyt}, measures the rate constant of electron transfer through the RC under steady-state conditions and can be expressed from rate constants of photochemistry, k_I, interquinone electron transfer, k_{AB}, and P^+ rereduction by reduced cytochrome *c*, k_c (eq 1) if other reactions (eqs 4 and 5) are not rate-limiting (Scheme 2):

$$\frac{1}{k_{cyt}} = \frac{1}{k_1} + \frac{1}{k_{AB}} + \frac{1}{k_c} \quad \text{(A16)}$$

The rate constant of P^+ rereduction depends on rates of binding of reduced cytochrome to the RC ($k_{on}[cyt^{2+}]$) and unbinding of oxidized cytochrome from the RC (k_{off}). As they are consecutive reactions

$$\frac{1}{k_c} = \frac{1}{k_{on}[cyt]} + \frac{1}{k_{off}} \quad \text{(A17)}$$

The "on" and "off" rate constants can be expressed by the ionic strength of the solution (*I*) and the ion exclusion radii of the interacting proteins RC (R_{RC}) and cytochrome (R_{cyt}) (see ref *41*):

$$k_{on} = k_{on}(I\rightarrow\infty)\left(\frac{k_{on}(I\rightarrow 0)}{k_{on}(I\rightarrow\infty)}\right)^{\alpha} \quad \text{(A18)}$$

$$k_{off} = k_{off}(I\rightarrow\infty)\left(\frac{k_{off}(I\rightarrow 0)}{k_{off}(I\rightarrow\infty)}\right)^{\alpha} \quad \text{(A19)}$$

where

$$\alpha = \frac{1}{2}\left(\frac{e^{-3.25\sqrt{IR_{RC}}}}{1+3.25\sqrt{IR_{cyt}}} + \frac{e^{-3.25\sqrt{IR_{cyt}}}}{1+3.25\sqrt{IR_{RC}}}\right) \quad \text{(A20)}$$

If the RC is partly inhibited by the bound transition metal ion, the observed rate constant of steady-state cytochrome photooxidation can be expressed by the weighted sum of the rate constants for native (n) and inhibited (i) RCs:

$$k_{cyt} = k_{cyt}(n)\frac{[RC]_t - [M{-}RC]}{[RC]_t} + k_{cyt}(i)\frac{[M{-}RC]}{[RC]_t} \quad \text{(A21)}$$

where the fraction of the RC in complex with metal ion can be expressed from eq A4:

$$\frac{[M{-}RC]}{[RC]_t} = \frac{\frac{I}{3} + [RC]_t + K_D - \sqrt{\left(\frac{I}{3} + [RC]_t + K_D\right)^2 - \frac{4}{3}[RC]_t I}}{2[RC]_t} \quad \text{(A22)}$$

Transition metal ions bound to the RC decrease k_{AB} only, and the inhibited value $k_{AB}(i)$ is taken as the fitting parameter in Figure 4 (see Table 3.)

REFERENCES

1. Blankenship, R. E., Madigan, M. T., and Bauer, C. E., Eds. (1995) *Anoxygenic Photosynthetic Bacteria*, Kluwer Academic Publishers, Dordrecht.
2. Wraight, C. A. (1998) in *Photosynthesis: Mechanisms and Effects* (Garab, Gy., Ed.) Vol. II, pp 693−698, Kluwer Academic Publishers, Dordrecht.
3. Mulkidjanian, A. Y. (1999) *FEBS Lett. 463*, 199−204.
4. Okamura, M. Y., Paddock, M. L., Graige, M. S., and Feher, G. (2000) *Biochim. Biophys. Acta 1458*, 148−163.
5. Kleinfeld, D., Okamura, M. Y., and Feher, G. (1984) *Biochim. Biophys. Acta 785*, 126−140.
6. Graige, M. S., Paddock, M. L., Bruce, J. M., Feher, G., and Okamura, M. Y. (1996) *J. Am. Chem. Soc. 118*, 9005−9016.
7. Graige, M. S., Feher, G., and Okamura, M. Y. (1998) *Proc. Natl. Acad. Sci. U.S.A. 95*, 11679−11684.
8. Maróti, P., and Wraight, C. A. (1988) *Biochim. Biophys. Acta 934*, 314−328.
9. Maróti, P., and Wraight, C. A. (1997) *Biophys. J. 73*, 367−381.
10. Wraight, C. A. (1979) *Biochim. Biophys. Acta 548*, 309−327.
11. Stowell, M. H. B., McPhillips, T. M., Rees, D. C., Soltis, S. M., Abresch, E., and Feher, G. (1997) *Science 276*, 812−816.
12. Brzezinski, P., Okamura, M. Y., and Feher, G. (1992) in *The Photosynthetic Bacterial Reaction Center II* (Breton, J., and Vermeglio, A., Eds.) pp 321−330, Plenum Press, New York.
13. Abresch, E. C., Paddock, M. L., Stowell, M. H. B., McPhillips, T. M., Axelrod, H. L., Soltis, S. M., Rees, D. C., Okamura, M. Y., and Feher, G. (1998) *Photosynth. Res. 55*, 119−125.
14. Gopta, O. A., Cherepanov, D. A., Junge, W., and Mulkidjanian, A. Y. (1999) *Proc. Natl. Acad. Sci. U.S.A. 96*, 13159−13164.
15. Miksovska, J., Schiffer, M., Hanson, D. K., and Sebban, P. (1999) *Proc. Natl. Acad. Sci. U.S.A. 96*, 14348−14353.
16. Cherepanov, D. A., Bibikov, S. I., Bibikova, M. V., Bloch, D. A., Drachev, L. A., Gopta, O. A., Oesterhelt, D., Semenov, A. Y., and Mulkidjanian, A. Y. (2000) *Biochim. Biophys. Acta 1459*, 10−34.
17. Shinkarev, V. P., and Wraight, C. A. (1993) in *The Photosynthetic Reaction Center* (Deisenhofer, J., and Norris, J., Eds.) Vol. I, pp 193−255, Academic Press, New York.
18. Okamura, M. Y., and Feher, G. (1995) in *Anoxygenic Photosynthetic Bacteria* (Blankenship, R. E., Madigan, M. T., and Bauer, C. E., Eds.) pp 577−594, Kluwer Academic Publishers, Dordrecht.
19. Ermler, U., Fritzsch, G., Buchanan, S. K., and Michel, H. (1994) *Structure 2*, 925−936.
20. Paddock, M. L., Rongey, S. H., Feher, G., and Okamura, M. Y. (1989) *Proc. Natl. Acad. Sci. U.S.A. 86*, 6602−6606.
21. Takahashi, E., and Wraight, C. A. (1990) *Biochim. Biophys. Acta 1020*, 107−111.
22. Takahashi, E., and Wraight, C. A. (1992) *Biochemistry 31*, 855−866.
23. Maróti, P., Hanson, D. K., Schiffer, M., and Sebban, P. (1995) *Nat. Struct. Biol. 2*, 1057−1059.
24. Sebban, P., Maróti, P., and Hanson, D. K. (1995) *Biochimie 77*, 677−694.
25. Tandori, J., Sebban, P., Michel, H., and Baciou, L. (1999) *Biochemistry 38*, 13179−13187.
26. Alexov, E. G., and Gunner, M. R. (1999) *Biochemistry 38*, 8253−8270.
27. Gunner, M. R., and Alexov, E. (2000) *Biochim. Biophys. Acta 1458*, 63−87.
28. Utschig, L. M., Ohigashi, Y., Thurnauer, M. C., and Tiede, D. M. (1998) *Biochemistry 37*, 8278−8281.
29. Utschig, L. M., Poluektov, O., Tiede, D. M., and Thurnauer, M. C. (2000) *Biochemistry 39*, 2961−2969.
30. Paddock, M. L., Graige, M. S., Feher, G., and Okamura, M. Y. (1999) *Proc. Natl. Acad. Sci. U.S.A. 96*, 6183−6188.
31. Paddock, M. L., Feher, G., and Okamura, M. Y. (2000) *Proc. Natl. Acad. Sci. U.S.A. 97*, 1548−1553.
32. Axelrod, H. L., Abresch, E. C., Paddock, M. L., Okamura, M. Y., and Feher, G. (2000) *Proc. Natl. Acad. Sci. U.S.A. 97*, 1542−1547.
33. Axelrod, H. L., Abresch, E. C., Paddock, M. L., Okamura, M. Y., and Feher, G. (2000) *Biophys. J. 78*, A337.
34. Overfield, R. E., and Wraight, C. A. (1986) *Photosynth. Res. 9*, 167−179.
35. Moser, C. C., and Dutton, P. L. (1988) *Biochemistry 27*, 2450−2461.
36. Tiede, D. M., Vashishta, A. C., and Gunner, M. R. (1993) *Biochemistry 32*, 4515−4531.
37. Van Gelder, B. F., and Slater, E. C. (1962) *Biochim. Biophys. Acta 58*, 593−595.
38. Stein, R. R., Castellvi, A. L., Bogacz, J. P., and Wraight, C. A. (1984) *J. Cell Biochem. 24*, 243−259.
39. Osváth, Sz., and Maróti, P. (1997) *Biophys. J. 73*, 972−982.
40. Larson, J. W., Wells, T. A., and Wraight, C. A. (1998) *Biophys. J. 74*, A76.
41. Gerencsér, L., Laczkó, G., and Maróti, P. (1999) *Biochemistry 38*, 16866−16875.
42. Kálmán, L., and Maróti, P. (1994) *Biochemistry 33*, 9237−9244.
43. Graige, M. S., Paddock, M. L., Feher, G., and Okamura, M. Y. (1999) *Biochemistry 38*, 11465−11473.
44. Wyman, J., and Gill, S. J. (1990) *Binding and Linkage: Functional Chemistry of Biological Macromolecules*, University Science Books, Mill Valley, CA.
45. Beatty, J. T., Paddock, M. L., Feher, G., and Okamura, M. Y. (2000) *Biophys. J. 78*, A339.
46. Rabenstein, B., Ullmann, G. M., and Knapp, E. W. (1998) *Eur. Biophys. J. 27*, 626−637.
47. Paddock, M. L., Rongey, S. H., McPherson, P. H., Juth, A., Feher, G., and Okamura, M. Y. (1994) *Biochemistry 33*, 734−745.
48. Nabedryk, E., Breton, J., Hienerwadel, R., Fogel, C., Mäntele, W., Paddock, M. L., and Okamura, M. Y. (1995) *Biochemstry 34*, 14722−14732.
49. Takahashi, E., and Wraight, C. A. (1991) *FEBS Lett. 283*, 140−144.
50. Maróti, P., Hanson, D. K., Baciou, L., Schiffer, M., and Sebban, P. (1994) *Proc. Natl. Acad. Sci. U.S.A. 91*, 5617−5621.
51. Takahashi, E., and Wraight, C. A. (1996) *Proc. Natl. Acad. Sci. U.S.A. 93*, 2640−2645.

BI0021636